

Artificial Photosynthesis with Semiconductor–Liquid Junctions

Néstor Guijarro, Florian Le Formal, and Kevin Sivula*

Abstract: Given the urgent need to develop a sustainable, carbon neutral energy storage system on a global scale, intense efforts are currently underway to advance the field of artificial photosynthesis: *i.e.* solar fuel engineering. In this review we give an overview of the field of artificial photosynthesis using a semiconductor–electrolyte interface employed in a photoelectrochemical device or as a heterogeneous photocatalyst. First we present a basic description of the operation principles of a semiconductor–liquid junction based device. The role of nanotechnology in the recent advances in the field is highlighted and common material systems under current study are briefly reviewed. The importance of the material surfaces are further scrutinized by presenting recent advances in interfacial engineering. Technical challenges and an outlook towards industrialization of the technology are given.

Keywords: Energy storage · Hydrogen · Nanoparticles · Photoelectrochemical water splitting · Semiconductor · Solar fuels · Thin films

1. Introduction

Illumination from the Earth's largest renewable energy source, the Sun, is sufficient to cover the energy requirements of human society many times over. However, because sunshine is locally periodic and variable, a sustainable energy economy based on solar energy cannot be realized until a method to efficiently convert, safely store and transport this energy is available at a scale commensurate with the global energy economy. Storing solar energy chemically in the form of covalent bonds, *i.e.* producing solar fuels *via* photosynthesis, is especially attractive for this purpose, given that the infrastructure for the widespread use of fossil fuels is already in place. Indeed, since the perpetuation of natural (biological) photosynthesis over millions of years resulted in the formation of the fossil fuels we employ today, a photosynthesis-based sustainable energy economy is an evident solution. However, the ability to rely solely on natural photosynthesis and the so-called biofuels has been called into question due to the inability to raise the photosynthetic efficiency and yields of useful products beyond the threshold that constitutes commercial viability. Indeed, the metabolic engineering required to advance this field remains a

difficulty as altering cellular biochemistry to generate biofuel product(s) involves no incentive for the organism, whose priorities are growth and competitive survival, rather than helping to solve energy-related problems in the human economy.^[1]

While efforts to increase the conversion efficiency of photosynthetic organisms are ongoing, and biofuels will certainly play a role in a future sustainable energy economy, a favorable alternative is to engineer artificial systems capable of stable and efficient photosynthesis. In this short review, we give an overview of the field of artificial photosynthesis using a semiconductor–electrolyte interface employed in a photoelectrochemical device or as a heterogeneous photocatalyst. A basic description of the operation principles of a semiconductor–liquid junction based device is given before common material systems under current study are briefly reviewed. Recent advances in interfacial engineering highlight the importance of the surface. Technical challenges and an outlook towards industrialization of the technology are given at the end. First, we discuss the motivation for the development of artificial photosynthetic (photoelectrochemical) technology in the framework of other solar energy conversion devices.

2. Motivation and Theoretical Background

2.1 Routes to Synthetic Fuels from Solar Energy

An obvious method to harvest solar energy for any purpose is to use the heat that results from matter absorbing solar irradiation.

This photon-to-phonon (or vibrational motion) conversion with concentrated solar power may be used to drive thermochemical reactions to split carbon dioxide to carbon monoxide or to split water to make hydrogen.^[2] These products can be further used in Fischer–Tropsch type processes to make methane and higher order hydrocarbons. Many thermochemical cycles have been suggested,^[3] for example using a metal/metal oxide as intermediate, and this class of solar energy conversion will also most likely play a role in a future sustainable energy economy. Drawbacks to this technology include the identification of materials that can withstand the high temperatures required and the fact that high conversion efficiency is only possible at a large scale. This diminishes the possibility to have small or medium scale distributed conversion systems. Moreover, the technology is best suited for geographical areas with high levels of insolation. Diffuse sunlight due to cloud cover is generally not sufficient to drive solar thermal installations and passing clouds can cause thermal transients that put added stress on the materials employed.^[4]

On the other hand, photovoltaic (PV) technology, wherein solar photons are converted directly to electrical energy, is a familiar example of a distributed and easily scalable solar energy technology. To achieve artificial photosynthesis, PV can be combined with an electrochemical cell for the electrosynthesis of solar fuels *via* the reduction of water into hydrogen, or of CO₂ into formate, CO, or methanol. To complete a reaction in an electrochemical cell, the fuel-producing reduction reactions must occur with a corresponding oxidation

*Correspondence: Prof. K. Sivula
École Polytechnique Fédérale de Lausanne
Institute of Chemistry and Chemical Engineering
CH H4 565, Station 6
CH-1015 Lausanne
Tel.: +41 21 693 7979
E-mail: kevin.sivula@epfl.ch

reaction, which is most conveniently water oxidation to produce O_2 and H^+ as both H_2O and CO_2 reduction require protons. A simple schematic of a closed energy cycle using an artificial photosynthesis device that splits water into H_2 and O_2 is shown in Fig. 1. Here a fuel cell could be used to convert the energy stored in the H_2 back into electricity on demand. Alternatively the H_2 can be converted to higher molecular weight liquid fuels using the reverse water gas shift (producing CO from CO_2) followed by a Fischer–Tropsch type process. The combustion of the liquid hydrocarbon fuel would return CO_2 to the atmosphere in a carbon-neutral cycle.

Despite the apparent ease of artificial photosynthesis offered by the PV + electrolysis approach, an important and general drawback comes from the operation of a traditional solar cell like those based on the silicon pn-junction. The voltage output of a pn-junction is strongly dependent on the illumination intensity. This necessitates complicated switching mechanisms to ensure the optimum number of cells are connected in series during variations in light intensity caused by haze, cloud cover, or time of day. This drawback can result in a significant energy loss up to 50%. Moreover, the cost of the fuel produced by this method is generally limited by the price and availability of traditional PV. Estimates vary widely, but a reasonable number is around 10 USD kg^{-1} H_2 for the combination of silicon PV and a polymer electrolyte membrane (PEM) electrolyzer to produce H_2 via water reduction.^[5] Since this price is much higher than the current price of H_2 obtained via the steam reforming of methane (ca. 1 USD kg^{-1}), there is little industrial motivation to adopt this technology. However, because the development of a hydrogen based energy economy based on solar water splitting remains a promising goal, researchers have

been inspired to develop systems for artificial photosynthesis that could potentially be radically less expensive than the traditional PV + electrolysis approach. In particular, employing a direct semiconductor–liquid junction in a photoelectrochemical (PEC) device can significantly simplify the overall solar-to-fuel process and potentially make solar fuel devices considerably more economically feasible, compared to the currently available technology.^[6] Indeed, PEC solar fuel production has been a promising possibility ever since the seminal demonstration of water photolysis on TiO_2 by Fujishima and Honda in 1972.^[7] Next we summarize the operation principle of artificial photosynthesis with a semiconductor–liquid junction.

2.2 An Ideal Semiconductor–Liquid Junction

In natural biological photosynthesis, solar photons are harvested by molecular chromophores (e.g. chlorophyll) wherein a solar photon excites an electron from the ground state to a distinct, localized, and unoccupied energy state at higher energy. In contrast to these discrete energy states, in crystalline solid-state materials the electron energy levels are so dense that they form broad bands of allowed energy separated by gaps of forbidden energies. A semiconductor is a material with an energy gap, E_g , of ca. 1–4 eV between the band of states occupied with electrons (the valence band) and the band that is vacant (at absolute zero, the conduction band). An incident solar photon can be absorbed by a semiconductor material if the energy of the photon, $h\nu$, is greater than the band gap energy, E_g . This absorption event accordingly promotes an electron from the valence band to the conduction band. Capturing the energy of this excited state before the promoted electron recombines with its electron-hole (the vacancy created in the

valence band) therein lies the challenge for solar energy conversion with semiconductors in general.

An important thermodynamic quantity, which describes the chemical potential (free energy) for electrons in a solid-state material, is the Fermi level, E_F . For semiconductors, E_F can be considered to be a hypothetical energy level of an electron, such that at thermodynamic equilibrium this energy level would have a 50% probability of being occupied at any given time. By doping the semiconductor (i.e. introducing impurity atoms that either donate electrons to, or accept them from, the valence electron configuration of the material), the Fermi energy will move closer to the conduction band (for donating impurities, n-type doping) or closer to the valence band (for accepting impurities, p-type doping). Fig. 2a illustrates this schematically by showing the change in energy of a semiconductor in a vacuum at ambient temperature after p-doping. Here the impurity atoms (not shown) have accepted electrons making them negatively charged and resulting in an E_F close to the valence band. The absence of valence band electrons due to their capture by the dopant atoms, results in an increased concentration of electron holes, which can be considered as positively-charged carriers (quasi particles) in their own right. It is important to note that the remaining electron holes balance the charge of the dopant atoms and make the material electronically neutral. While a rigorous mathematical description of the electronics of semiconductors is available elsewhere,^[8] and the idealisms presented are only strictly valid for single crystal semiconductors, with these basic concepts we can begin to assemble an ideal semiconductor–liquid junction for artificial photosynthesis.

In a liquid redox electrolyte the electrochemical potential of electrons, E_{redox} , is related by the Nernst expression to the ratio of concentrations of the oxidized and reduced species in the redox couples present. While E_{redox} and E_F are both thermodynamic free energies of electrons, care must be taken to directly compare their values as different references potentials are traditionally used. In semiconductor physics, the energy of an electron in a vacuum is typically referenced while electrochemists typically use the normal hydrogen electrode (NHE). NHE, which implies an electrolyte pH of 0, lies about -4.5 eV from the vacuum level as is shown in Fig. 2b.^[9] Before immersing a semiconductor in a liquid electrolyte, it can be assumed that $E_{redox} \neq E_F$ as the two phases are not yet in equilibrium with each other. Upon contact equilibration occurs through the transfer of electrons from the phase with electrons with higher energy to the one with a lower

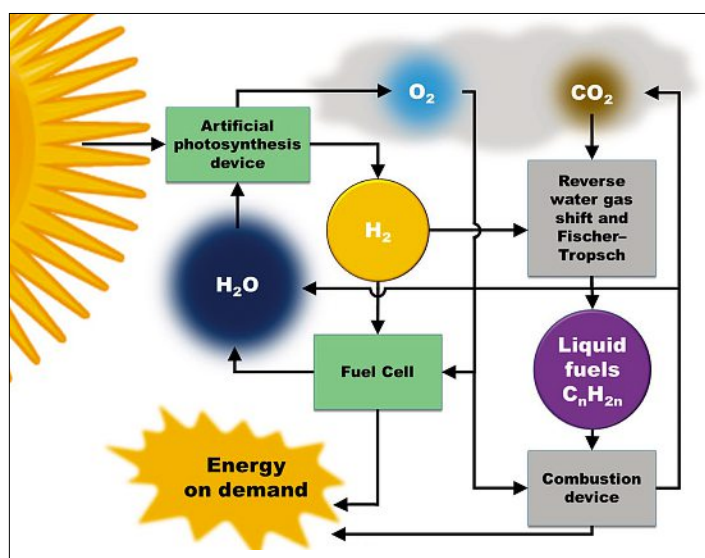


Fig. 1. A simplified schematic of a closed carbon-neutral energy cycle using an artificial photosynthesis device that splits water into H_2 and O_2 . Hydrogen can be stored and used when needed in a fuel cell or combined with CO_2 to make liquid fuels.

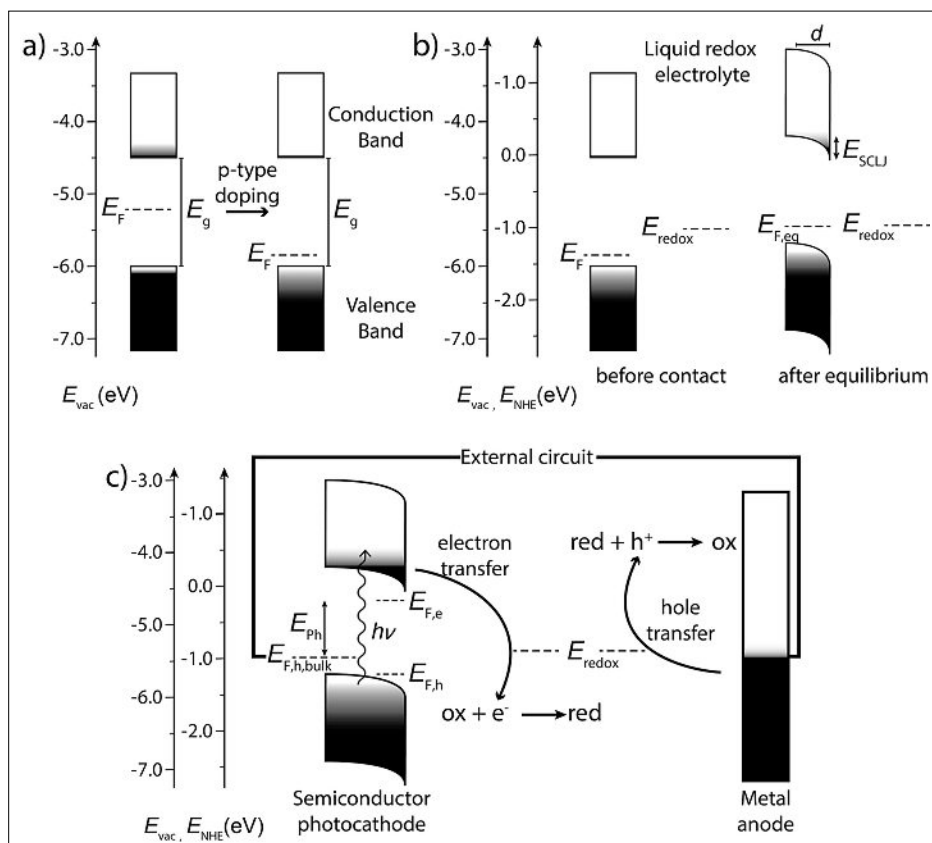


Fig. 2. a) An intrinsic semiconductor with the important parameters E_F and E_g indicated. The p-type doping of a semiconductor with electron accepting impurities leads to the decrease in E_F , pushing it closer to the valence band. b) The interfacing of a p-type semiconductor with a liquid electrolyte results in the band bending and the development of a depletion zone, d . c) A complete photoelectrochemical cycle where a metal anode is electrically connected to the p-type photocathode. Upon photon absorption a splitting of the Fermi level occurs giving electron, $E_{F,e}$, and hole, $E_{F,h}$, quasi-Fermi levels and a photoelectrochemical potential, E_{ph} .

energy. This is shown in Fig. 2b for a p-type semiconductor with $E_{redox} > E_F$ before equilibrium. Here electrons flow from the electrolyte into the semiconductor, raising the electron free energy until an equilibrium value, $E_{F,eq}$, is reached. This process results in a band-bending and a built-in potential, E_{SCLJ} , at the semiconductor–liquid junction (SCLJ). This can be rationalized by, instead of thinking about electron transfer, considering that (positively charged) holes are transferred from the semiconductor into the electrolyte, leaving the (spatially fixed) negatively charge impurities behind over a certain distance into the semiconductor film, d , called the depletion width (this space is free of majority charge carriers, so it is also called the space charge layer). The band bending in the depletion layer comes with an electric field, which is a key aspect to harvesting solar energy. A more complete description of this equilibrium process is given in ref. [10] and we note that in many ways it is similar to the more familiar Schottky junction that can form at a semiconductor–metal junction.

Upon the absorption of a photon in the depletion layer of the semiconductor, the electric field drives the separation of the

electron-hole pair. For the p-type semiconductor the electron will move to the SCLJ and the hole will drift into the bulk. Under continuous illumination electrons can accumulate at the interface and raise the local free electron energy, creating a new quasi Fermi-level for electrons, $E_{F,e}$. The difference between the quasi Fermi-level for electrons at the interface and the Fermi-level for holes in the bulk of the semiconductor, $E_{F,eq}$, is the photopotential generated by the electrode, E_{ph} . Under the right conditions, if there is an overlap of the density of available states in the redox couple and $E_{F,e}$, electron transfer can occur from the semiconductor to reduce the oxidized species of the redox couple. In a practical artificial photosynthesis device this would be reducing water to H_2 or CO_2 to CO. In the complete PEC cell, both a reduction and an oxidation reaction must occur. In our example with a p-type semiconductor acting as a (photo)cathode and performing the reduction reaction, the oxidation reaction will occur at the anode using the electron holes that have drifted into the bulk, and diffused to the back contact and through an external circuit in to the anode. This is shown in Fig. 2c. An analogous

process can occur with a semiconductor photoanode and a (metal) cathode.

Overall it is the inherent simplicity of this single semiconductor device that can potentially reduce the cost of PEC solar fuel production over the traditional PV+electrolysis approach. However, one challenge has been to identify a material that has suitable properties for the stable solar water splitting or CO_2 reduction with high efficiency. Indeed, while the redox potentials of water reduction and oxidation imply that a semiconductor with a minimum E_g of 1.23 eV should be sufficient, the thermodynamic limitation of developing E_{ph} as high as E_g and kinetic overpotentials, η_{ox} and η_{red} , for the oxidation and reduction reactions, require that E_g is at least 2.3 eV. In practice only materials with $E_g > 3.0$ eV have been shown to be reliably able to supply sufficient potential to drive both the reduction and oxidation reactions for water splitting. This precludes the semiconductor from absorbing an appreciable amount of solar energy, as most photons are in the 1.5–2.5 eV range. To overcome this issue, and the fact that no one material has the ideal band edge energy levels, a tandem cell approach^[11] can be used with

only a minimal increase in system complexity (and potential manufacturing cost). Here a photocathode and a photoanode are used together to generate sufficient photopotential to drive both redox reactions and also harness a sufficient portion of the solar energy. This device is shown conceptually for water splitting in Fig. 3. Based on a recent theoretical assessment, the potential solar-to-fuel conversion efficiency is over 20% with $E_g \approx 1.9$ and 1.4 eV respectively for the first and second photoelectrodes.^[11] This approach also allows more flexibility in the choice for E_g 's to achieve maximum theoretical solar-to-fuel conversion over 10%. Importantly, a recent technoeconomic analysis suggested that if a 10% efficient device could be produced for around 150 USD m^{-2} the solar fuel produced would be economically competitive with the traditional approach.^[12] Thus a major challenge has been the identification of robust but also inexpensive materials and processing techniques to afford photoelectrodes for a low-cost tandem cell.

2.3 Nanostructured and Nanoparticle Electrodes

Before mentioning the materials employed for artificial photosynthesis using semiconductor–liquid junctions it is important to note that very significant advances in the field of semiconductor-based photoelectrochemistry have been enabled in the past decade by the advent of nanotechnology. Nanostructuring semiconductor electrodes has proven to hold the key to further tune the optical/electronic properties

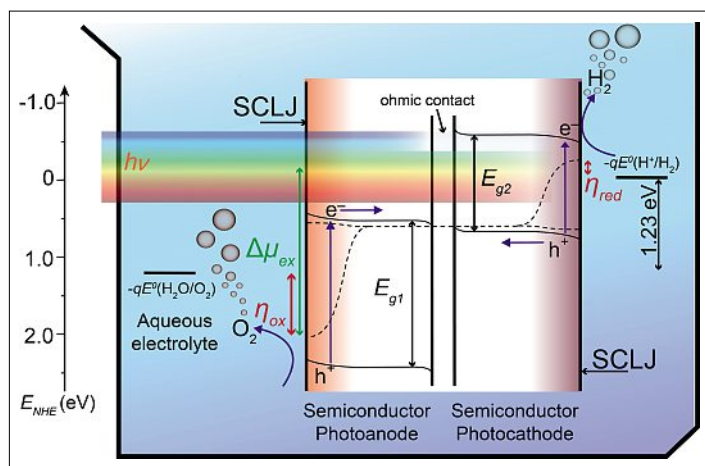


Fig. 3. Electron energy scheme of PEC water splitting using a dual-absorber tandem cell. The combination of two absorbers as shown will increase the free energy ($\Delta\mu_{ex}$) available. This free energy must be greater than the energy needed for water splitting (1.23 eV) plus the overpotential losses at both the anode and the cathode, η_{ox} and η_{red} , for the water splitting reaction to occur. Four photons must be absorbed in this mechanism to produce one molecule of H_2 . Reprinted with permission from ref. [11]. Copyright 2013 The American Chemical Society.

of the materials, circumventing the inherent carrier transport limitations of several bulk materials, and therefore, enhancing the photocatalytic performance compared to the starting 'bulk' materials. Broadly speaking, nanostructuring semiconductor electrodes entails the transition from single crystal or polycrystalline materials that display the classical planar semiconductor-liquid junction (SCLJ, see above), to nanoscaled geometries, *i.e.* nanoparticles, nanorods, nanowires, *etc.* that afford a high-surface area three-dimensional interface. In such a way, whereas most of the semiconductor material remains far from the SCLJ in the planar configuration, the open structure and high surface-to-volume ratio of nanostructured films allows the electrolyte to permeate the entire film. The difference in the SCLJ geometry has dramatic implications not only on the active surface area of the electrodes but also on the photogenerated carrier dynamics (*i.e.* charge separation and recombination).

In contrast to planar SCLJs where the space charge layer drives the charge separation, in nanocrystalline systems, the crystal size is commonly so small that the band bending is negligible. In fact, given that the width of the space charge layer can be larger than the size of the crystals and that the mobile ions in the permeating electrolyte can neutralize any electric field, a depletion layer can often not be borne in the nanocrystals. In this situation, once carriers (electrons and holes) are photogenerated inside the semiconductor, one of them is preferentially transferred to the electrolyte (corresponding to the minority carrier) whereas the other (majority carrier) would be preferentially transported

towards the collector.^[13] Thus this type of device is based on the kinetic competition between charge transfer/transport and recombination.^[8,14] Although one-dimensional structures (*viz.* nanorods or nanotubes) display some degree of directionality on charge collection, transport in nanoparticulate systems are defined by the 'random walk' model, particle-to-particle hopping or electron tunneling, which are generally accompanied by higher resistance and recombination in grain boundaries.^[15] Consequently, in nanostructured semiconductors the relative electron/hole injection rates to the electrolyte together

with the applied potential pulling the carriers to the rear collector dictate the charge separation, and even in some cases, modulate the n- or p-type photoelectrochemical behavior of the electrodes.^[16]

Regarding the effect of the increased surface area of the semiconductor-liquid junction, the yield of the oxidation/reduction reaction relies on the ability of the photogenerated carriers (electrons and holes) to reach the interface at the electrolyte or at the rear contact. The charge transport properties depend on the material, the carrier type and the light intensity. While in the absence of an electric (space charge) field, the charges can travel by diffusion only, the nanostructuring can shorten the distance the minority carriers have to diffuse to reach the SCLJ while maintaining the overall thickness of the film, which potentially can reduce the recombination and enhance the performance. However, it is important to note that surface-related recombination pathways of photogenerated carriers can also be enhanced because of the surface enlargement.^[15]

Given the success of nanostructured electrodes, a prevailing device design that incorporates this concept together with the tandem cell idea is shown in Fig. 4a.^[17] Here the two semiconductors are electrically connected in a transparent membrane that would be impermeable to H_2 and O_2 but would allow H^+ (or OH^-) ion transfer. The semiconductors are envisioned to be wires that have diameters on the nanometer length scale to reduce the distance for minority carriers to and distribute charge-carriers over a larger area to reduce catalyst turnover requirements. The one-dimensional form of the nanowires can further

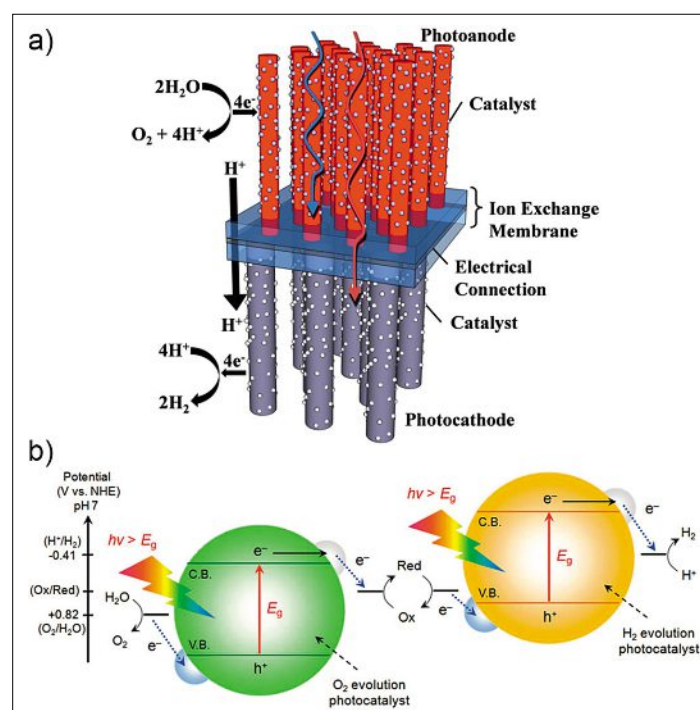


Fig. 4. a) A schematic of a proposed artificial photosynthesis device incorporating the tandem concept and nanowire semiconductor arrays as explained in the main text. Reprinted from ref. [17]. Copyright 2011 The Royal Society of Chemistry. b) A schematic energy diagram of particulate photocatalytic water splitting by a two-step (tandem) photoexcitation system. Reprinted from ref. [18]. Copyright 2010 The American Chemical Society.

facilitate the transport of majority carriers, and allow space for ion transfer across the membrane. H_2 would be collected on the cathode side and O_2 could be vented to the atmosphere from the anode side.

2.4 Particulate Semiconductor Approach

An ultimate step towards maximizing the specific surface area of the SCLJ involves the removal of the electrodes completely and simply dispersing the semiconductor material as nano- or microparticles in the liquid electrolyte. In such a manner, problems of charge transport can be circumvented. Indeed it is estimated that this approach could produce H_2 at one tenth of the cost compared to the electrode based system using materials with the same efficiency and lifetime.^[12] However, the main limitation of this system lies in the slow transfer kinetics of the charge transfer step. As mentioned above, given the small particle size needed for a stable dispersion, an internal mechanism to separate photogenerated carriers (a space charge) does not exist, and only the relative electron/hole injection rates into the electrolyte govern the charge separation. In nanostructured films carriers can delocalize and move away from each other which lengthen the carrier lifetimes, but in suspended particles charges remain confined in a nanometer distance, which promotes their recombination. In this scenario charge recombination strongly competes with charge separation limiting the yield of energy conversion.^[19] In fact, strategies to promote charge separation like surface decoration with co-catalysts that are known to participate in charge extraction/collection^[20] and enhance the kinetics for water reactions or the use of sacrificial reagents have been demonstrated to improve the photocatalytic activity.^[18,19] In addition the tandem concept can also be employed here by using two types of particulate photocatalysts and an intermediate redox couple as shown in Fig. 4b. While the particulate approach is certainly promising given its low cost to implement, electrode-based devices will have to be first developed in order to more easily characterize the performance of the materials employed.

3. Promising Semiconductor Materials

Ever since the discovery of photoelectrochemical water splitting,^[7] a wide variety of materials have been investigated to this purpose. According to the basic mechanism of photocatalytic and photoelectrochemical water splitting the semiconductor materials should ideally meet the following conditions: (1) strong light absorption, (2)

chemical stability in aqueous solution both in dark and under illumination, (3) suitable band edge positions to enable water oxidation and reduction, (4) efficient charge transport, (5) low overpotential for the reactions and (6) low cost. Unfortunately, to date no material fulfilling all these requirements is known. The tandem cell concept discussed in section 2.2 does allow the search to be extended to materials that can perform either water reduction or oxidation, and many promising materials have been identified. In the following sections the main advances in oxides, chalcogenides and sensitized systems for photocatalytic and photoelectrochemical water splitting will be reviewed. As the energy of the conduction and valence bands and the band gap energy are the most relevant parameters of these materials, approximate values for these quantities (at pH 0) for the materials that will be discussed are shown in Fig. 5. Progress with these materials is most commonly quantified by the photocurrent density (in $mA\ cm^{-2}$) delivered by a photoelectrode at standard testing conditions. The photocurrent corresponds to the number of photogenerated carriers per unit area that are participating in the water reduction or water oxidation reactions. The onset of the photocurrent is also an important metric for operation in the tandem cell.^[11] This value is typically given versus the reversible hydrogen electrode (RHE), which is related to the NHE by the following expression: $E_{RHE} = E_{NHE} - 0.059 \cdot pH$.

3.1 Oxides

Semiconductor oxides have attracted much attention mostly because of their robustness towards the harsh conditions that accompany the photocatalytic/photoelectrochemical water splitting.

3.1.1 TiO_2

Ever since the pioneering work of Fujishima and Honda,^[7] extensive investigations have been devoted to this material.^[13a,21] While earlier works dealt with single-crystalline n-type TiO_2 ,^[7,22] recent advances have demonstrated the potential

of surface nanostructuring and modification to enhance the catalytic activity, and doping to extend the limited spectral response of the pristine material ($E_g = 3.0$ – $3.2\ eV$);^[13a] despite the large E_g of TiO_2 it cannot perform overall unassisted water splitting. Although the potential of the valence band edge is well below the water oxidation potential, the potential of the conduction band lies just slightly positive of the water reduction potential. Therefore, photogenerated electrons are not able to reduce the water in bias-free conditions, unless a gradient of pH or an external bias is applied.^[6] Its use in a tandem cell is ultimately limited by the small portion of the solar spectrum that can be harvested by this material.

Despite this, to date different TiO_2 nanostructures have been explored, viz. nanoparticulate films, nanorods and nanotubes arrays and branched nanorods, among others. In fact, direct comparison of these configurations in similar photoelectrochemical conditions reveals that the performance improves dramatically from nanoparticulate films to nanorods and branched-nanorods.^[23] Additionally, Jankuloska *et al.* recently reported an improvement to TiO_2 nanotube performance by decorating the surface with TiO_2 nanowires.^[24] These results suggest that directionality in electron transport for one-dimensional structures together with the high surface area of hierarchical architectures can enhance the photoelectrochemical response.

In order to extend the spectral response of TiO_2 towards the visible region, nitrogen- or hydrogen-doping have been reported. Nakamura *et al.* demonstrated that nitrogen-doped TiO_2 powder extend the photocurrent response from the UV-region ($< 400\ nm$) to the visible ($< 550\ nm$).^[25] The results were rationalized with the appearance of an N-induced mid-gap level slightly above the VB edge. Hoang *et al.* demonstrated that N-doping TiO_2 and cobalt incorporation as a co-catalyst can shift the spectral response from $420\ nm$ up to $550\ nm$ reaching incident photon to

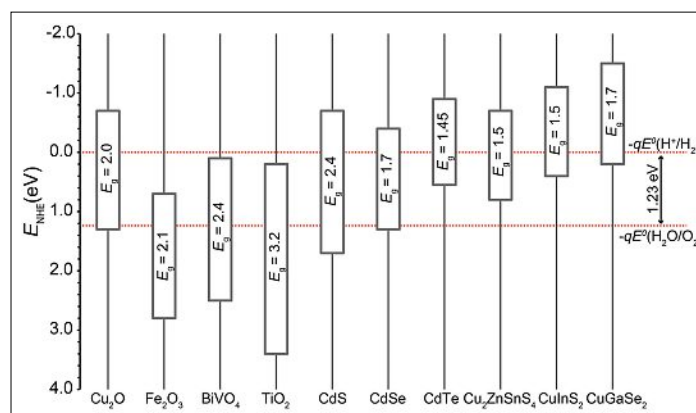


Fig. 5. The position of the conduction and valence bands and the band gap energy for selected promising semiconducting materials for artificial photosynthesis compared to the water reduction and oxidation potentials at pH 0.

current efficiency (IPCE) values of 18% at 450 nm.^[26] Hydrogenation of TiO₂ in H₂ atmosphere has been reported to create oxygen vacancy sites forming donor states below the conduction band, which improves the light absorption, charge transport and, thus, the water oxidation performance.^[27] In fact, the doped H:TiO₂ nanowires have reached incident photon to current efficiency (IPCE) values of ~40% at 400 nm, compared to only 4% for the pristine sample.^[28] Additionally, given the mismatch position of the conduction band energy to perform unassisted water splitting, surface treatment with 'interface conditioners' have been proposed as a manner to tune the bands position and/or passivate surface-related recombination.^[13a] To date, the most studied have been fluoride,^[29] phosphate^[30] or neutral organophosphonated molecules,^[13a] among others. The long-term stability of these band-gap tuned TiO₂ derivatives is one area of interest towards the practical application of this material.

3.1.2 Fe₂O₃

Contrary to TiO₂, α -Fe₂O₃ (hematite) exhibits a lower band gap (~2.0 eV) which allows for a better light harvesting, and while this material is very stable in basic electrolyte, early studies with polycrystalline samples revealed its major weaknesses, namely, low charge carrier mobility, slow water oxidation kinetics and short photogenerated carrier lifetime.^[15,31] However, different strategies such as doping, surface nanostructuring and modifications have proved quite successful in boosting the photoelectrochemical response of this material. First attempts to prepare Fe₂O₃ nanostructures used the spray pyrolysis technique,^[32] which was later optimized by Grätzel's group.^[33] In this case, serendipitous incorporation of silicon as dopant demonstrated a drastic enhancement of the photoelectrochemical performance promoting fractal morphologies.^[34] As subsequently proved by Le Formal *et al.*, the silicon doping affects the nucleation and growth mechanism of the hematite, promoting higher crystallinity.^[35] Similarly, underlayers of Nb₂O₃ and Ga₂O₃ were demonstrated to enhance the photocurrent in a similar way.^[36] Films of nanostructured Fe₂O₃ have also been prepared by doctor blading and thermal annealing 'inks' of Fe₂O₃ nanoparticles.^[37] In this case, thermal annealing at 800 °C was shown to be critical to enhance the photoelectrochemical response mainly because of the efficient particle necking and, presumably, Sn⁴⁺ doping that diffuses into the hematite from the substrate. While the particle size was too large for high photocurrent given the necking and sintering at 800 °C, using SiO₂ as an encapsulant for

the Fe₂O₃ prior to annealing (and removing after) led to improved photocurrents values, which was attributed to the higher surface area.^[38] More recently, the ultimate benchmark on the performance of hematite photoelectrodes has been achieved by Kim *et al.* for a Pt-doped single-crystalline worm-like architecture, reaching photocurrents of 4.32 mA cm⁻² at 1.23 V vs RHE.^[39] However, as 12.6 mA cm⁻² are possible given the light absorption of this material,^[31] more optimization of the performance is possible.

3.1.3 BiVO₄

This ternary compound exhibits a band gap of 2.4 eV, but similar to Fe₂O₃, the conduction band edge lies well below the water reduction potential. Therefore, it requires an electrical or chemical bias to perform overall water splitting if it is not used in a tandem system.^[6] Turner and co-workers reported on Mo-doped BiVO₄ nanostructured films prepared by metal-organic decomposition, whose performance was more than doubled by the surface modification with cobalt-phosphate (Co-Pi) as co-catalyst for OER.^[40] More recently, Van de Krol's group optimized a spray pyrolysis technique to prepare nanostructured films.^[41] Interestingly, they found that an absorbed photon to current efficiency (APCE) close to unity is obtained under low irradiance, showing that the main limitation on the material is the carrier transport and the slow water oxidation kinetics at the surface. In order to improve charge transport and enhance the kinetics of the oxygen evolution reaction, W was introduced as a dopant and the surface was modified with Co-Pi, achieving a photocurrent of 2.3 mA cm⁻² (at 1.23 V vs RHE), which surpasses the 1.7 mA cm⁻² previously reported for the undoped sample.^[41] Very recently, gradient W-doping of BiVO₄ was reported as a way to further enhance the charge transport.^[42] In this case, photocurrent values of ~2 mA cm⁻² were already reported at 0.5 V vs RHE, where negligible values were previously reported and 3.5 mA cm⁻² were achieved at 1.23 V vs RHE.

3.1.4 Cu₂O

Cuprous oxide is a p-type semiconductor with a band gap energy of 2.0 eV, whose conduction band edge is well located to perform water reduction, lying 0.7 V negative of the water reduction potential, and the valence band edge is just slightly positive of the water oxidation potential (without enough overpotential to drive the water oxidation reaction in the absence of an external bias) thus it is commonly considered as a photocathode for the tandem cell.^[6] While this semiconductor can be easily prepared by thermal oxidation, sputtering, or electrodeposition, it is prone

to photocorrosion in aqueous conditions. Recently, Paracchino *et al.* demonstrated that protecting the Cu₂O film with conformal layers of TiO₂ and Al:ZnO keeps the Cu₂O protected from the water, and including Pt as a catalyst photocurrent values close to 8 mA cm⁻² and an onset of photocurrent of 0.4 V vs RHE were attained, though stability tests reveals photocorrosion or catalyst detachment after few minutes.^[43] Afterwards, different catalysts like MoS₂ or RuO₂ combined with steam-annealing treatments demonstrated improved lifetime of the electrodes for several days without significant losses.^[44] It is not clear if the protecting layers could afford stability for the desired 10 year lifetime.

3.2 Chalcogenides

Application of semiconductor chalcogenides in the field of solar-to-energy conversion, especially photovoltaics, has been fueled by their outstanding optoelectronic properties. Crystalline materials can be synthesized at lower temperatures compared to a typical oxide and their optoelectronic properties can be easily tuned by leveraging quantum confinement effect. However, most of these materials suffer severe photocorrosion in aqueous medium, which raises serious concerns on their actual application for water splitting.

3.2.1 Binary Chalcogenides

Among binary chalcogenides CdS, CdSe and CdTe have been interrogated as photocatalysts for water splitting. CdS is an n-type semiconductor with a band gap of 2.4 eV whose conduction band edge and valence band edge straddle the water oxidation and reduction potentials to perform overall water splitting.^[45] However, given the fast photocorrosion of CdS in the absence of a sacrificial hole scavenger,^[46] only studies of H₂ evolution are reported.^[47] Note that few reports employed overlayers of conductive polymers to extract the holes and transport them to the electrolyte surface circumventing the CdS degradation.^[48] Generally nanoparticles of CdS modified with a co-catalyst for HER (viz. Pt, MoS₂, Ru) are suspended in an aqueous medium containing a sacrificial hole acceptor (S²⁻, SO₃²⁻, etc.).^[47a] CdSe is another n-type semiconductor with a band gap energy of 1.7 eV that has been reported to perform photocatalytic H₂ evolution in certain conditions, *i.e.* for nanosized particles and in the presence of co-catalyst and sacrificial hole acceptors.^[49] Osterloh and co-workers demonstrated that whereas bulk CdSe was unable to perform water reduction because of the conduction band edge location, nanosized-CdSe, with a higher conduction band position (due to quantum confinement), was active for photocatalytic H₂ evolution.^[50] Likewise,

Han *et al.* reported a CdSe nanocrystals dispersion that in the presence of Ni-based co-catalyst and sacrificial hole scavengers was able to produce H₂. CdTe, exhibiting a band gap energy of 1.44 eV, has been recently targeted as a photoanode for water oxidation.^[51] Lichterman *et al.* reported an n-CdTe film protected by a layer of amorphous 'leaky' TiO₂ deposited by ALD and decorated with NiO co-catalyst, obtaining saturated photocurrents of ~20 mA cm⁻².^[52] In this case the overlayer of TiO₂ protects and passivates the CdTe while providing a channel for photogenerated holes to reach the interface with the electrolyte.

3.2.2 Ternary/quaternary Chalcogenides

Semiconductor p-type materials like CuInS₂, CuGaSe₂, CuIn_xGa_{1-x}Se₂ or Cu₂ZnSnS₄ have been scrutinized as photocathodes for water photoreduction. To date, most of the investigations have been developed with polycrystalline films deposited by electrodeposition or vacuum deposition techniques. In all the cases, creation of a p-n junction was proven to be necessary to extract photogenerated carriers from the active layer.^[53] Generally, a layer n-type CdS (buffer layer) of a few tens of nanometers is chemically-deposited on top of the active layer, prior co-catalyst deposition. Ikeda *et al.* first reported the use of CuInS₂ as photocathode with a bandgap of 1.5 eV for water reduction reaching IPCE values around 20% in the visible range.^[54] Lately, Domen and co-workers optimized CuInS₂ deposition and employed In₂S₃ as buffer layer attaining IPCE values close to 40%.^[55] and very recently, an electrodeposited porous CuInS₂ photocathode delivered IPCE values close to 60% in the visible range, and photocurrent density of 14 mA cm⁻².^[56] However, there are serious concerns about the stability of these systems as emphasized in the corresponding reports. An overlayer of TiO₂ deposited on top of the CdS has been reported to improve the stability and performance. CuInGaSe₂ films and Cu₂ZnSnS₄ polycrystalline films have proven to deliver very high photocurrents close to 10 mA cm⁻².^[57] Likewise, suspended Cu₂ZnSnS₄ nanocrystals decorated with Pt or Au have proven to generate H₂ under illumination and in the presence of sacrificial hole scavengers.^[58] CuGaSe₂ with a band gap energy of 1.68 eV have emerged as one of the most promising chalcogenides delivering IPCE values close to 50% with proved stability for more than 10 days in the absence of any protecting layer.^[59] More recently, Domen's group, in pursuit of improving photogenerated charge extraction, modified the (Ag,Cu)GaSe₂ photocathode with a thin layer of CuGa₃Se₅, prior depositing CdS and Pt.^[60] In such a way IPCE values

close to 60%, and, more importantly, onset of photocurrent of 1 V vs RHE, were obtained. To date, few reports deal with the use of nanostructured architectures, and in these cases, photoelectrochemical measurements are mostly reported in the presence of electron scavenger species and poor performances are still observed. The reason may arise from the absence of a strong particle sintering, which causes critical recombination losses at particle-particle interfaces.^[53,61] Annealing at high temperatures causes dramatic degradation of the materials (oxidation under air and decomposition under inert atmosphere).

3.3 Hybrid Oxide-Dye Approach

In view of the impressive performance of the dye-sensitized solar cells (DSSCs), where photogenerated carriers generated in a dye attached to a mesoporous TiO₂, are rapidly separated by injection in TiO₂ (electron) and redox species of the electrolyte (hole), several groups attempted to extend this concept to photoelectrochemical water oxidation.^[62] Notably, this approach more closely resembles natural photosynthesis given its use of carbon-based chromophores. An organic dye with a LUMO level more negative than the conduction band edge of TiO₂ (to ensure electron injection) and a HOMO level more positive than the water oxidation redox potential can be employed. Note that given the slow kinetics for water oxidation, co-catalyst particles, like IrO_x, are included in the system, either directly grafted to the dye or deposited in the TiO₂ near the dye.^[63] Photocurrents delivered by this systems (tens of μA cm⁻²) are far from those recorded in photovoltaic operation conditions, emphasizing the enhanced carrier recombination given the poor hole extraction kinetics. Likewise, inverted configuration was employed to directly generated H₂, *i.e.* sensitizing a mesoporous NiO that plays the role of hole acceptor and using cobalt-based as co-catalyst.^[64] However, both photocathode and photoanode based oxide sensitization have delivered very poor performances up to now. Alternatively, dyes have been substituted by semiconductor nanocrystals displaying better performances. In fact, Yang *et al.* recently reported a photocathode based on ZnS-coated CdS-sensitized TiO₂ decorated with IrO_x and a photoanode based on ZnS-coated CdSe-sensitized NiO decorated with NiS, both delivering stable photocurrents of around 200 μA cm⁻².^[65]

4. Engineering Semiconductor Interfaces

While the control of nanostructure, as discussed above, has brought significant

progress to the performance of photoelectrode for artificial photosynthesis, the increased surface area of the semiconductor amplifies the problems associated with interfaces (*e.g.* defect and trapping states). Moreover, several factors besides band gap and energy band positions may limit the employment of a material in a water splitting device. These factors include notably stability, interfacial recombination and poor charge transfer to the electrolyte. The semiconductor electrolyte interface plays an essential role in these aspects, as we have already seen through some of the examples discussed above. In this section, the specific strategies developed to overcome surface limitations are presented and discussed individually.

4.1 Anti-Corrosion Coatings

In the previously mentioned reports regarding the development of cuprous oxide, Cu₂O, for photoelectrochemical water reduction,^[43,44] the corrosion of the semiconductor was avoided using a protective overlayer to prevent the direct contact of the semiconductor and the electrolyte. This was accomplished by depositing wide band gap, stable materials by Atomic Layer Deposition (ALD) to ensure a conformal coating. In addition to offering stability, such overlayers can also facilitate charge extraction through the formation of a buried p-n junction.^[66] Similar strategies have been employed to protect other semiconductor materials commercially used in the PV industry and considered for application in artificial photosynthesis. N-type silicon electrodes, utilized as water oxidation photoanodes, were stabilized with ALD grown TiO₂ overlayers, pin-hole free but sufficiently thin to allow charge tunneling.^[67] Alternatively, this type of photoanode has also been coated, using the same ALD technique, with cobalt oxide that acts simultaneously as a protecting layer and a catalyst.^[68] As TiO₂ is a wide band gap semiconductor and is therefore transparent to 96% of the standard solar spectrum, it can serve as a suitable protective layer without competing for light absorption. It has also been used to protect p-type silicon, gallium arsenide (GaAs) and gallium phosphide (GaP), all employed as photocathodes for water reduction.^[69] The conductivity of such TiO₂ layers has been carefully investigated as thick layers of ALD TiO₂, potentially required to fully cover the surface of the photoelectrode, can result in electronic losses due to its high resistivity. However, increasing the donor density by vacuum annealing^[70] or controlling the defect density that can act as charge hopping sites in amorphous titania ('leaky' TiO₂)^[69a,71] can reduce these losses and increase the charge transfer though the passivating overlayer.

4.2 Overlayers for Assisting Charge Separation and Stability

As mentioned in section 3, the application p-type materials like CuInS_2 , CuGaSe_2 , $\text{CuIn}_x\text{Ga}_{1-x}\text{Se}_2$ or $\text{Cu}_2\text{ZnSnS}_4$ in artificial photosynthesis require surface treatment in order to observe water reduction photocurrents. These n-type overlayers (e.g. CdS) can be combined with wide band gap oxides to afford both improved charge extraction and stability. For example, in a recent study by Rovelli *et al.*^[72] $\text{Cu}_2\text{ZnSnS}_4$ deposited by either a sequential or a simultaneous electrodeposition method on Mo substrates was investigated with different combinations of overlayers (Fig. 6). Interestingly while the p-n junction seems to be effective in the $\text{Cu}_2\text{O}/\text{AZO}/\text{TiO}_2$ electrodes discussed above, the $\text{CZTS}/\text{AZO}/\text{TiO}_2$ did not show photoactivity (green curves, Fig. 6). The presence of the CdS overlayer was found to be essential for photocurrent, however, electrodes with the CZTS/CdS structure were found to be poorly stable and the photocurrents diminished quickly during linear scanning (from positive to negative) potentiometry measurements under intermittent illumination (red curves, Fig. 6). The combination of both CdS and AZO/TiO_2 overlayers were found to provide both charge extraction and stable photocurrents of reasonable magnitude (black curves, Fig. 6). In addition to CdS other n-type overlayers (e.g. CdSe, ZnSe, and In_2S_3)^[53,55,60] have been identified as suitable for charge extraction layers. However, simplification of the system by identifying one overlayer that could provide both charge extraction and stability would help reduce the complexity and potential cost of this class of electrodes.

4.3 Catalyst for Hydrogen Evolution and Oxygen Evolution

The optimization of photoelectrodes for the several tasks required by artificial photosynthesis, notably light absorption, charge transport and chemical reaction catalysis, is challenging. To enhance the latter role, photocathodes and photoanodes are typically modified on their surface with a catalyst layer. Some catalysts were mentioned in section 3 with respect to different materials. Here we add that the ideal hydrogen evolution reaction (HER) and oxygen evolution (OER) catalysts for PEC water splitting need to operate at low overpotentials and also should be optically transparent and form a stable electrical contacts with the photoabsorbing material.^[6]

Platinum, the best HER catalyst as observed experimentally and supported by theoretical calculations,^[73] is often deposited on a photocathode to promote hydrogen production (e.g. as in the previous example with CZTS). Surface decoration

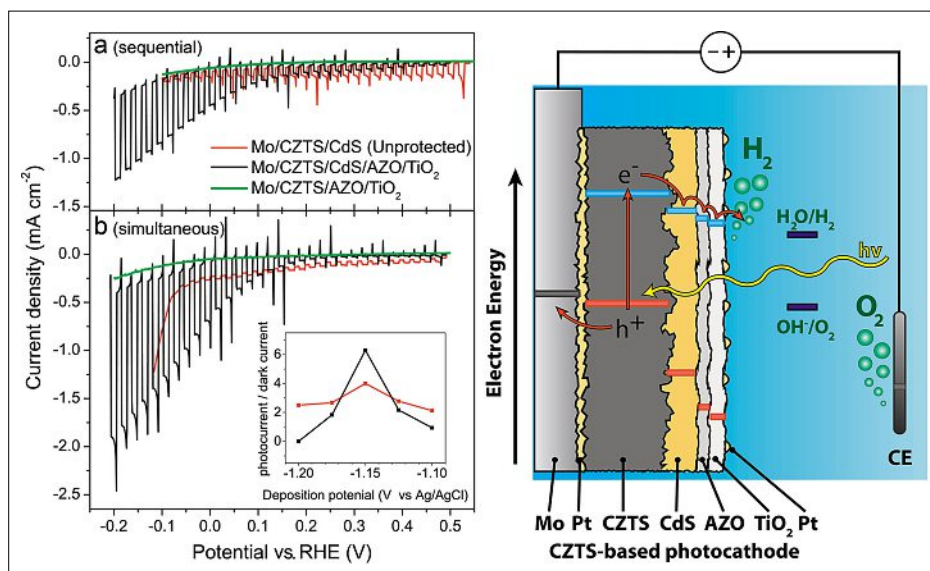


Fig. 6. Linear sweep voltammograms under chopped light illumination for the sequentially (a) and simultaneously (b) deposited CZTS-based films, with and without the ALD protective layer (AZO/TiO_2) or the CdS layer. All measurements were carried out at pH 7. The inset of (b) shows the photoactivity (expressed as the ratio of photocurrent to dark current) of the CZTS/CdS cells as a function of the potential applied during simultaneous electrodeposition. Photoactivity was assessed by linear sweep voltammetry: current values were taken at 0.2 V vs. Ag/AgCl at pH 9 for unprotected samples (for stability reasons) and at 0 V vs. RHE at pH 7 for protected samples. Reprinted with permission from ref. [72]. Copyright 2013 The American Chemical Society.

with Pt nanoparticles is commonly carried out by either photodeposition or electrodeposition, by applying a constant potential in a solution containing H_2PtCl_6 . Likewise, other methods such as impregnation with the solution of H_2PtCl_6 followed by annealing in reducing atmospheres or even ALD have been also reported. Such surface treatment has been performed on protected silicon,^[74] CZTS,^[75] Cu_2O ^[43] or TiO_2 nanoparticles.^[76] However, platinum is scarce and costly for large scale application.^[44a] Additionally, the weak adhesion of this catalyst onto the photocathode has been assumed to cause desorption of the nanoparticles and loss of photoactivity after only a few hours.^[44b]

Because of these drawbacks, alternative earth-abundant catalysts are under intense examination. MoS_2 has been shown to be stable in a wide range of pH and to exhibit similar performance as Pt on ALD protected cuprous oxide, but with improved stability.^[44a] Similarly, the effect was also observed on p-type silicon photocathode coated with TiO_2 ,^[77] RuO_x and Ni-Mo nanoparticles are also currently under investigation for the same purpose.^[44b,78]

In contrast to most photocathodes, oxygen evolving photoanodes based on transition metal oxide semiconductors can produce photocurrent corresponding to the oxygen evolution reaction without a catalyst overlayer.^[35,79] Nevertheless, deposition of an OER catalyst atop the photoactive layer enhances in most cases the performance of the photoanode, with a

cathodic shift of the onset potential and/or an increase in photocurrent density. Cobalt based oxides and hydroxides are one of the most frequently used catalysts for oxygen evolution. Simple deposition methods such as drop casting a cobalt nitrate solution onto an iron oxide electrode lead to a cathodic shift of 50 mV for the photocurrent.^[34a] Other cobalt compounds, like a cobalt phosphate (CoPi)^[80] that can be (photo-)electrodeposited on the surface, exhibit a gain of more than 100 mV on the same semiconductor and on BiVO_4 .^[41,81] The improved performance of the CoPi over other cobalt-based overlayers is supposedly caused by a thicker and more porous structure of the catalyst.

Improvement of the photoanode performance has also been obtained using iridium oxide nanoparticles but the poor stability of this material in mild to basic pH limits its utilization for oxides, which are typically stable in alkaline media.^[82] Recently, significant progress has been obtained using novel catalyst materials. For example, the photocurrent onset potential of a bismuth vanadate electrode has been shifted to a value close to the theoretical value (the flat band potential) using a dual $\text{FeOOH}/\text{NiOOH}$ catalyst layer.^[83] Analogously, the onset potential of iron oxide photoanode has been reduced by more than 300 mV using a NiFeO_x composite,^[84] prepared by sol-gel and drop casted onto a thin hematite electrode.^[85]

While the improvement of the photoactivity observed with the Co-based and

NiFeO_x overlayers is clearly demonstrated by the PEC performance, the source of improvement is not yet fully understood.^[86] Spectroscopic studies have evidenced that the photogenerated holes are still detected in hematite when covered with cobalt phosphate although longer lived.^[87] Moreover, the higher photovoltage, detected on Fe₂O₃/NiFeO_x electrodes as compared to bare electrodes has been rationalized in terms of suppression of Fermi level pinning.^[85] These two studies suggest that these ‘catalyst’ layers do not accelerate the reaction kinetics but rather decrease the surface recombination losses.

4.4 Suppression/Reduction of Surface Recombination

Hematite is one of the most studied photoanodes for water photo-oxidation, and while photocurrents over 3–4 mA cm⁻² are routinely found under standard testing conditions, the photocurrent onset potential is usually around 1.0 V vs. RHE. The observed onset is in stark contrast with the theoretical onset, the flat band potential, which has been determined around 0.4–0.5 V vs RHE,^[88] suggesting a large 500 mV loss. As discussed previously, these losses can be reduced by 10% with the deposition of a ‘catalyst’ layer such as a CoO_x overlayer. However, another type of surface treatment has evidenced a positive effect on the reduction of the voltage losses. The coating of nanostructured hematite photoanodes with a very thin layer (0.1 to 2 nm) of alumina by ALD results in a significant shift of the photocurrent onset by 100 mV.^[89] Further investigation by spectroscopic techniques has provided evidence that the cathodic shift is rather due to the passivation of surface trapping states (reduction of surface recombination) than increased reaction rate. Furthermore, the improvement due to the surface passivation was enhanced when subsequently covering the surface with CoO_x, leading to an overall cathodic shift of 150 mV (Fig. 7). This study shows that both surface recombination and slow water oxidation kinetics can be overcome using a combination of two layers with two different roles. However, the overpotential losses were still not completely eliminated. Thus additional overlayers have since been investigated. Notably a similar passivation effect was observed when covering the hematite surface with a 13-group oxide using chemical bath deposition, particularly Ga₂O₃.^[90] Ga₂O₃ and Al₂O₃ are structural isomorphs of hematite but are commonly known to be more stoichiometric, *i.e.* richer in oxygen. Therefore the passivation of surface oxygen vacancies, which can create Fe²⁺ species acting as surface traps, is the prevailing explanation for the improvement offered by these overlayers.

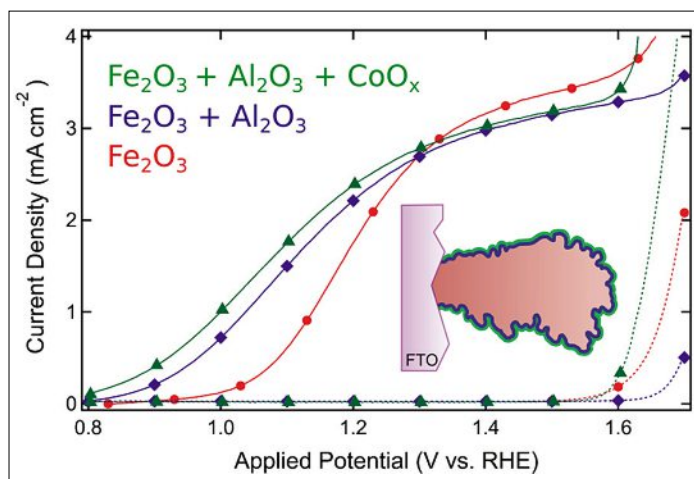


Fig. 7. Current densities (in mA cm⁻²) of nanostructured Fe₂O₃ photoanodes in the dark (broken lines) and under simulated solar illumination are shown as a function of the applied potential (V vs. RHE) with the different surface treatments as indicated. The inset scheme represents the nanostructured hematite photoanode covered with a surface passivation layer (Al₂O₃) and a catalyst (CoO_x). FTO stands for the F:SnO₂ transparent conductive substrate. Adapted from ref. [89].

In general, the study and characterization of potential surface traps on semiconductor photoelectrodes has been one area of particular interest. Additional evidence of surface states on Fe₂O₃ photoanodes has been collected through the observation of charge trapping in spectroscopic studies. Interfacial charge accumulation has been characterized using transient photocurrent and photovoltage,^[91] whereas the surface capacitance engendered by the charge accumulation has been detected by frequency modulated techniques, such as photo-electrochemical impedance spectroscopy^[92] or intensity modulated photocurrent spectroscopy.^[93] These studies have highlighted the charge trapping on the surface, showed its reduction when using a passivating overlayer, and demonstrated the very slow kinetics of the water oxidation (*ca.* 1 s). Due to this long timescale, positive charges accumulate on the SCLJ and are assumed to cause ‘back electron recombination’, with electrons diffusing from the bulk through the space charge layer to recombine with holes waiting at the interface with water.^[94]

Overall, it is clear that the deposition of multiple overlayers onto photoactive semiconductors is an effective strategy to overcome surface limitations. Nonetheless, these overlayers can bring additional concerns such as electronic and optical losses in case of non-optimized junctions or inappropriate material properties. Therefore, a future goal in the field is to find a single layer that can combine all the properties that counteract detrimental surface processes, leading to a substantial increase in performance for water splitting photocathode and/or photoanode.

5. Complete Device Demonstrations

While much work in the past decade has been devoted to enhancing the performance of individual photoelectrodes for application to artificial photosynthesis, important progress has also been made in assembling complete devices for overall solar-to-chemical conversion. A seminal demonstration was made by Khaselev and Turner with their monolithic (p-GaInP₂/GaAs cells) photovoltaic-photoelectrochemical device for hydrogen production.^[95] This architecture attained 12.4% solar-to-hydrogen conversion efficiency. However, the high cost and the poor stability of the device renders it impractical for commercial application. Since this demonstration there has been many reports of photovoltaic–photoelectrochemical tandem type cells with CIGS,^[96] amorphous silicon,^[42] dye sensitized,^[97] and other types of photovoltaic devices. We point the reader to a recent review for more information.^[11] However, given the need to encapsulate the PV part of the device, it is not clear that the photovoltaic–photoelectrochemical approach could meet the *ca.* \$150 m⁻² cost target. Less work has been performed on the photoanode–photocathode tandem cell, but some demonstrations have been made. For example, p-type CaFe₂O₄ (*E_g* = 1.9 eV), has been paired with n-TiO₂ (in a side-by-side configuration) to give an unassisted operating photocurrent of 110 μA cm⁻² in 0.1 M NaOH electrolyte with the light from a 500 W Xe lamp.^[98] However, only 12% of the current observed was due to water splitting and Fe and Ca were detected in

the electrolyte after the device test, suggesting corrosive side reactions were occurring. P-type nanotubular Cu-Ti-O films were also paired with TiO₂ to give a working tandem device with a photocurrent of 0.25 mA cm⁻² (solar-to-hydrogen conversion around 0.30%) under standard illumination conditions. However, this system only demonstrated a stability in the time-scale of minutes.

More recently Bornoz *et al.* combined a BiVO₄ photoanode with a Cu₂O photocathode and employing water oxidation and reduction catalysts (Co-Pi and RuO_x, respectively) to show that an unassisted solar photocurrent density on the order of 1 mA cm⁻² was possible in a tandem cell.^[99] Different thicknesses of the BiVO₄ were also used to probe the effect of light transmission to the Cu₂O electrode. Photocurrents corresponding to *ca.* 0.5% solar-to-hydrogen conversion efficiency were found to decay over the course of minutes because of the detachment of the Co-Pi catalyst (Fig. 8).

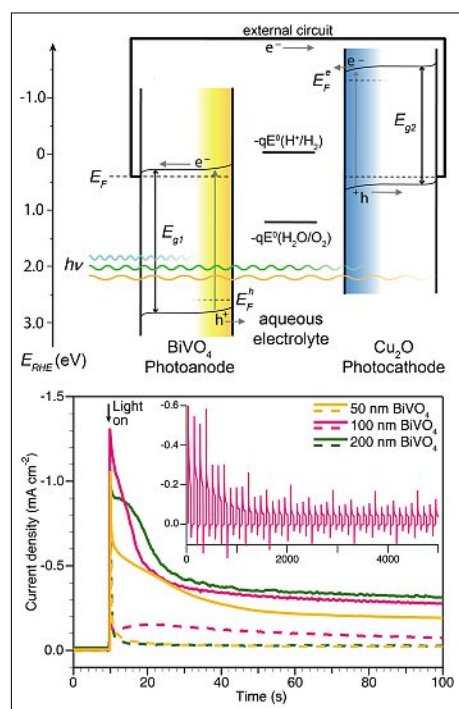


Fig. 8. (Top) Simplified electron energy diagram of a bismuth vanadate photoanode/cuprous oxide photocathode tandem cell for overall water splitting. (Bottom) Two-electrode Cu₂O/BiVO₄ tandem cell transient current density curves with (solid lines) and without (dashed lines) the cobalt catalyst applied. Simulated solar illumination (100 mW cm⁻²) was activated after 10 seconds in the dark. The inset shows an extended transient current density curve for the tandem cell constructed with the 100 nm BiVO₄ photoanode under light chopping conditions (60 s light on, 60 s light off). Reprinted with permission from ref. [99]. Copyright 2014 The American Chemical Society.

6. Conclusion and Outlook

In this short review we have presented the motivation and the theoretical framework for artificial photosynthesis using a direct semiconductor–liquid junction. While the elegance and simplicity of this approach could potentially lead to a device that can convert solar energy directly into chemical energy at a cost that is significantly less than the traditional photovoltaic + electrolyzer approach, challenges remain for the commercial application of this technology. Many materials have been identified with appropriate attributes that can be improved using nanotechnology. Engineering the interfaces by applying buffer layers for charge extraction, trap passivation, corrosion protection, and catalysts has aided drastically the performance of photoelectrodes prepared with inexpensive semiconductor materials.

Future work is most needed to identify better suited semiconductor materials (improved stability p-type materials, and n-type materials with low photocurrent onset potentials), and in the development of inexpensive deposition techniques to keep the manufacturing cost as low as possible. Indeed techniques like atomic layer deposition, which has been discussed extensively in this review, are not likely to be suitable for the *ca.* \$150 m⁻² cost target for large area devices. Furthermore, it is expected that the development of a tandem cell approach will eventually extend to the realization of a highly efficient particulate photocatalyst system that will store energy from the sun as chemical bonds for a fraction of the cost of an electrode based system, and bring to fruition a sustainable energy economy based on artificial photosynthesis.

Received: December 9, 2014

- [1] A. Melis, *Energy Environ. Sci.* **2012**, 5, 5531.
- [2] a) T. Kodama, N. Gokon, *Chem. Rev.* **2007**, 107, 4048; b) L. Xiao, S.-Y. Wu, Y.-R. Li, *Renew. Energ.* **2012**, 41, 1.
- [3] M. Roeb, M. Neises, N. Monnerie, F. Call, H. Simon, C. Sattler, M. Schmücker, R. Pitz-Paal, *Materials* **2012**, 5, 2015.
- [4] G. Augsburg, D. Favrat, *Sol. Energy* **2013**, 87, 42.
- [5] a) N. R. C. Committee on Alternatives and Strategies for Future Hydrogen Production and Use, National Academy of Engineering, 'The Hydrogen Economy: Opportunities, Costs, Barriers, and R&D Needs', National Academies Press, Washington, **2004**; b) T. L. Gibson, N. A. Kelly, *Int. J. Hydrogen Energy* **2008**, 33, 5931
- [6] M. G. Walter, E. L. Warren, J. R. McKone, S. W. Boettcher, Q. Mi, E. A. Santori, N. S. Lewis, *Chem. Rev.* **2010**, 110, 6446.
- [7] A. Fujishima, K. Honda, *Nature* **1972**, 238, 37.
- [8] R. Krishnan, in 'Encyclopedia of Electrochemistry', Wiley-VCH Verlag GmbH & Co. KGaA, **2007**.
- [9] S. Trasatti, *Pure Appl. Chem.* **1986**, 58, 955.
- [10] R. Memming, 'Semiconductor Electrochemistry', Wiley-VCH, **2001**.
- [11] M. S. Prévot, K. Sivula, *J. Phys. Chem. C* **2013**, 117, 17879.
- [12] B. A. Pinaud, J. D. Benck, L. C. Seitz, A. J. Forman, Z. Chen, T. G. Deutsch, B. D. James, K. N. Baum, G. N. Baum, S. Ardo, H. Wang, E. Miller, T. F. Jaramillo, *Energy Environ. Sci.* **2013**, 6, 1983.
- [13] a) T. Berger, D. Monllor-Satoca, M. Jankulovska, T. Lana-Villarreal, R. Gómez, *ChemPhysChem* **2012**, 13, 2824; b) G. Hodes, I. D. J. Howell, L. M. Peter, *J. Electrochem. Soc.* **1992**, 139, 3136.
- [14] A. Hagfeldt, M. Grätzel, *Chem. Rev.* **1995**, 95, 49.
- [15] F. E. Osterloh, *Chem. Soc. Rev.* **2013**, 42, 2294.
- [16] a) S. Ogawa, K. Hu, F.-R. F. Fan, A. J. Bard, *J. Phys. Chem. B* **1997**, 101, 5707; b) N. Guijarro, T. Lana-Villarreal, R. Gomez, *Chem. Commun.* **2012**, 48, 7681.
- [17] J. M. Spurgeon, M. G. Walter, J. Zhou, P. A. Kohl, N. S. Lewis, *Energy Environ. Sci.* **2011**, 4, 1772.
- [18] K. Maeda, K. Domen, *J. Phys. Chem. Lett.* **2010**, 1, 2655.
- [19] T. Hisatomi, J. Kubota, K. Domen, *Chem. Soc. Rev.* **2014**, 43, 7520.
- [20] A. Yamakata, M. Kawaguchi, N. Nishimura, T. Minegishi, J. Kubota, K. Domen, *J. Phys. Chem. C* **2014**, 118, 23897.
- [21] M. Ni, M. K. H. Leung, D. Y. C. Leung, K. Sumathy, *Renew. Sust. Energ. Rev.* **2007**, 11, 401.
- [22] A. J. Nozik, *Nature* **1975**, 257, 383.
- [23] I. S. Cho, Z. Chen, A. J. Forman, D. R. Kim, P. M. Rao, T. F. Jaramillo, X. Zheng, *Nano Lett.* **2011**, 11, 4978.
- [24] M. Jankulovska, I. Barceló, T. Lana-Villarreal, R. Gómez, *J. Phys. Chem. C* **2013**, 117, 4024.
- [25] R. Nakamura, T. Tanaka, Y. Nakato, *J. Phys. Chem. B* **2004**, 108, 10617.
- [26] S. Hoang, S. Guo, N. T. Hahn, A. J. Bard, C. B. Mullins, *Nano Lett.* **2011**, 12, 26.
- [27] G. Wang, H. Wang, Y. Ling, Y. Tang, X. Yang, R. C. Fitzmorris, C. Wang, J. Z. Zhang, Y. Li, *Nano Lett.* **2011**, 11, 3026.
- [28] S. Hoang, S. P. Berglund, N. T. Hahn, A. J. Bard, C. B. Mullins, *J. Am. Chem. Soc.* **2012**, 134, 3659.
- [29] H. Park, W. Choi, *J. Phys. Chem. B* **2004**, 108, 4086.
- [30] D. Zhao, C. Chen, Y. Wang, H. Ji, W. Ma, L. Zang, J. Zhao, *J. Phys. Chem. C* **2008**, 112, 5993.
- [31] K. Sivula, F. Le Formal, M. Grätzel, *ChemSusChem* **2011**, 4, 432.
- [32] K. Itoh, J. O. M. Bockris, *J. Electrochem. Soc.* **1984**, 131, 1266.
- [33] A. Duret, M. Grätzel, *J. Phys. Chem. B* **2005**, 109, 17184.
- [34] a) A. Kay, I. Cesar, M. Grätzel, *J. Am. Chem. Soc.* **2006**, 128, 15714; b) I. Cesar, A. Kay, J. A. G. Martinez, M. Grätzel, *J. Am. Chem. Soc.* **2006**, 128, 4582.
- [35] F. Le Formal, M. Grätzel, K. Sivula, *Adv. Funct. Mater.* **2010**, 20, 1099.
- [36] a) T. Hisatomi, H. Dotan, M. Stefik, K. Sivula, A. Rothschild, M. Grätzel, N. Mathews, *Adv. Mater.* **2012**, 24, 2699; b) T. Hisatomi, J. Brillet, M. Cornuz, F. Le Formal, N. Tetreault, K. Sivula, M. Grätzel, *Faraday Discuss.* **2012**, 155, 223.
- [37] K. Sivula, R. Zboril, F. Le Formal, R. Robert, A. Weidenkaff, J. Tucek, J. Frydrych, M. Grätzel, *J. Am. Chem. Soc.* **2010**, 132, 7436.
- [38] J. Brillet, M. Grätzel, K. Sivula, *Nano Lett.* **2010**, 10, 4155.
- [39] J. Y. Kim, G. Magesh, D. H. Youn, J.-W. Jang, J. Kubota, K. Domen, J. S. Lee, *Sci. Rep.* **2013**, 3, 2681.
- [40] S. K. Pilli, T. E. Furtak, L. D. Brown, T. G. Deutsch, J. A. Turner, A. M. Herring, *Energy Environ. Sci.* **2011**, 4, 5028.

- [41] F. F. Abdi, N. Firet, R. van de Krol, *ChemCatChem* **2013**, *5*, 490.
- [42] F. F. Abdi, L. Han, A. H. Smets, M. Zeman, B. Dam, R. van de Krol, *Nat. Commun.* **2013**, *4*, 2195.
- [43] A. Paracchino, V. Laporte, K. Sivula, M. Grätzel, E. Thimsen, *Nat. Mater.* **2011**, *10*, 456.
- [44] a) C. G. Morales-Guio, S. D. Tilley, H. Vrubel, M. Grätzel, X. Hu, *Nat. Commun.* **2014**, *5*, 3059; b) S. D. Tilley, M. Schreier, J. Azevedo, M. Stefiik, M. Grätzel, *Adv. Funct. Mater.* **2014**, *24*, 303.
- [45] A. Kudo, Y. Miseki, *Chem. Soc. Rev.* **2009**, *38*, 253.
- [46] M. J. Natan, J. W. Thackeray, M. S. Wrighton, *J. Phys. Chem.* **1986**, *90*, 4089.
- [47] a) X. Zong, H. Yan, G. Wu, G. Ma, F. Wen, L. Wang, C. Li, *J. Am. Chem. Soc.* **2008**, *130*, 7176; b) J. S. Jang, S. M. Ji, S. W. Bae, H. C. Son, J. S. Lee, *J. Photochem. Photobiol. A* **2007**, *188*, 112.
- [48] A. J. Frank, K. Honda, *J. Electroanal. Chem. Interfacial Electrochem.* **1983**, *150*, 673.
- [49] F. A. Frame, F. E. Osterloh, *J. Phys. Chem. C* **2010**, *114*, 10628.
- [50] F. Andrew Frame, E. C. Carroll, D. S. Larsen, M. Sarahan, N. D. Browning, F. E. Osterloh, *Chem. Commun.* **2008**, 2206.
- [51] Z. Han, F. Qiu, R. Eisenberg, P. L. Holland, L. D. Krauss, *Science* **2012**, *338*, 1321.
- [52] M. F. Lichterman, A. I. Carim, M. T. McDowell, S. Hu, H. B. Gray, B. S. Brunshwig, N. S. Lewis, *Energy Environ. Sci.* **2014**, *7*, 3334.
- [53] N. Guijarro, M. S. Prévot, K. Sivula, *J. Phys. Chem. Lett.* **2014**, *5*, 3902.
- [54] S. Ikeda, T. Nakamura, S. M. Lee, T. Yagi, T. Harada, T. Minegishi, M. Matsumura, *ChemSusChem* **2011**, *4*, 262.
- [55] G. Gunawan, W. Septina, S. Ikeda, T. Harada, T. Minegishi, K. Domen, M. Matsumura, *Chem. Commun.* **2014**, *50*, 8941.
- [56] J. Zhao, T. Minegishi, L. Zhang, M. Zhong, G. Gunawan, M. Nakabayashi, G. Ma, T. Hisatomi, M. Katayama, S. Ikeda, N. Shibata, T. Yamada, K. Domen, *Angew. Chem. Int. Ed.* **2014**, *53*, 11808.
- [57] a) D. Yokoyama, T. Minegishi, K. Maeda, M. Katayama, J. Kubota, A. Yamada, M. Konagai, K. Domen, *Electrochem. Commun.* **2010**, *12*, 851; b) D. Yokoyama, T. Minegishi, K. Jimbo, T. Hisatomi, G. Ma, M. Katayama, J. Kubota, H. Katagiri, K. Domen, *Appl. Phys. Exp.* **2010**, *3*, 101202.
- [58] X. Yu, A. Shavel, X. An, Z. Luo, M. Ibáñez, A. Cabot, *J. Am. Chem. Soc.* **2014**, *136*, 9236.
- [59] M. Moriya, T. Minegishi, H. Kumagai, M. Katayama, J. Kubota, K. Domen, *J. Am. Chem. Soc.* **2013**, *135*, 3733.
- [60] L. Zhang, T. Minegishi, M. Nakabayashi, Y. Suzuki, K. Seki, N. Shibata, J. Kubota, K. Domen, *Chem. Sci.* **2015**, in press.
- [61] S. C. Riha, S. J. Fredrick, J. B. Sambur, Y. Liu, A. L. Prieto, B. A. Parkinson, *ACS Appl. Mater. Interfaces* **2010**, *3*, 58.
- [62] S. Mathew, A. Yella, P. Gao, R. Humphry-Baker, B. F. E. Curchod, N. Ashari-Astani, I. Tavernelli, U. Rothlisberger, M. K. Nazeeruddin, M. Grätzel, *Nat. Chem.* **2014**, *6*, 242.
- [63] a) J. R. Swierk, T. E. Mallouk, *Chem. Soc. Rev.* **2013**, *42*, 2357; b) W. J. Younplblood, S. H. A. Lee, Y. Kobayashi, E. A. Hernandez-Pagan, P. G. Hoertz, T. A. Moore, A. L. Moore, D. Gust, T. E. Mallouk, *J. Am. Chem. Soc.* **2009**, *131*, 926.
- [64] L. Li, L. Duan, F. Wen, C. Li, M. Wang, A. Hagfeldt, L. Sun, *Chem. Commun.* **2012**, *48*, 988.
- [65] H. B. Yang, J. Miao, S.-F. Hung, F. Huo, H. M. Chen, B. Liu, *ACS Nano* **2014**, *8*, 10403.
- [66] A. Paracchino, N. Mathews, T. Hisatomi, M. Stefiik, S. D. Tilley, M. Grätzel, *Energy Environ. Sci.* **2012**, *5*, 8673.
- [67] Y. W. Chen, J. D. Prange, S. Dühnen, Y. Park, M. Gunji, C. E. D. Chidsey, P. C. McIntyre, *Nat. Mater.* **2011**, *10*, 539.
- [68] J. Yang, K. Walczak, E. Anzenberg, F. M. Toma, G. Yuan, J. Beeman, A. Schwartzberg, Y. Lin, M. Hettick, A. Javey, J. W. Ager, J. Yano, H. Frei, I. D. Sharp, *J. Am. Chem. Soc.* **2014**, *136*, 6191.
- [69] a) S. Hu, M. R. Shaner, J. A. Beardslee, M. Lichterman, B. S. Brunshwig, N. S. Lewis, *Science* **2014**, *344*, 1005; b) B. Seger, T. Pedersen, A. B. Laursen, P. C. K. Vesborg, O. Hansen, I. Chorkendorff, *J. Am. Chem. Soc.* **2013**, *135*, 1057.
- [70] B. Seger, S. D. Tilley, T. Pedersen, P. C. K. Vesborg, O. Hansen, M. Grätzel, I. Chorkendorff, *J. Mater. Chem. A* **2013**, *1*, 15089.
- [71] K. Sivula, *ChemCatChem* **2014**, *6*, 2796.
- [72] L. Rovelli, S. D. Tilley, K. Sivula, *ACS Appl. Mater. Interfaces* **2013**, *5*, 8018.
- [73] J. K. Nørskov, T. Bligaard, A. Logadottir, J. R. Kitchin, J. G. Chen, S. Pandelov, U. Stimming, *J. Electrochem. Soc.* **2005**, *152*, J23.
- [74] N. P. Dasgupta, C. Liu, S. Andrews, F. B. Prinz, P. Yang, *J. Am. Chem. Soc.* **2013**, *135*, 12932.
- [75] Y. Daisuke, M. Tsutomu, J. Kazuo, H. Takashi, M. Guijun, K. Masao, K. Jun, K. Hironori, D. Kazunari, *Appl. Phys. Exp.* **2010**, *3*, 101202.
- [76] J.-J. Zou, C.-J. Liu, K.-L. Yu, D.-G. Cheng, Y.-P. Zhang, F. He, H.-Y. Du, L. Cui, *Chem. Phys. Lett.* **2004**, *400*, 520.
- [77] B. Seger, A. B. Laursen, P. C. K. Vesborg, T. Pedersen, O. Hansen, S. Dahl, I. Chorkendorff, *Angew. Chem. Int. Ed.* **2012**, *51*, 9128.
- [78] C. G. Morales-Guio, L. Liardet, M. T. Mayer, S. D. Tilley, M. Grätzel, X. Hu, *Angew. Chem. Int. Ed.* **2014**, doi: 10.1002/anie.201410569.
- [79] Y. Ma, S. R. Pendlebury, A. Reynal, F. Le Formal, J. R. Durrant, *Chem. Sci.* **2014**, *5*, 2964.
- [80] M. W. Kanan, D. G. Nocera, *Science* **2008**, *321*, 1072.
- [81] D. K. Zhong, M. Cornuz, K. Sivula, M. Grätzel, D. R. Gamelin, *Energy Environ. Sci.* **2011**, *4*, 1759.
- [82] S. Tilley, M. Cornuz, K. Sivula, M. Grätzel, *Angew. Chem., Int. Ed.* **2010**, *49*, 6405.
- [83] T. W. Kim, K.-S. Choi, *Science* **2014**, *343*, 990.
- [84] R. D. L. Smith, M. S. Prévot, R. D. Fagan, Z. Zhang, P. A. Sedach, M. K. J. Siu, S. Trudel, C. P. Berlinguette, *Science* **2013**, *340*, 60.
- [85] C. Du, X. Yang, M. T. Mayer, H. Hoyt, J. Xie, G. McMahon, G. Bischofing, D. Wang, *Angew. Chem., Int. Ed.* **2013**, *52*, 12692.
- [86] D. R. Gamelin, *Nat. Chem.* **2012**, *4*, 965.
- [87] M. Barroso, C. A. Mesa, S. R. Pendlebury, A. J. Cowan, T. Hisatomi, K. Sivula, M. Grätzel, D. R. Klug, J. R. Durrant, *Proc. Nat. Acad. Sci.* **2012**, *109*, 15640.
- [88] I. Cesar, K. Sivula, A. Kay, R. Zboril, M. Grätzel, *J. Phys. Chem. C* **2009**, *113*, 772.
- [89] F. Le Formal, N. Tetreault, M. Cornuz, T. Moehl, M. Grätzel, K. Sivula, *Chem. Sci.* **2011**, *2*, 737.
- [90] T. Hisatomi, F. Le Formal, M. Cornuz, J. Brillet, N. Tetreault, K. Sivula, M. Grätzel, *Energy Environ. Sci.* **2011**, *4*, 2512.
- [91] F. Le Formal, K. Sivula, M. Grätzel, *J. Phys. Chem. C* **2012**, *116*, 26707.
- [92] B. Klahr, S. Gimenez, F. Fabregat-Santiago, T. Hamann, J. Bisquert, *J. Am. Chem. Soc.* **2012**, *134*, 4294.
- [93] L. M. Peter, K. G. U. Wijayantha, A. A. Tahir, *Faraday Discuss.* **2012**, *155*, 309.
- [94] F. Le Formal, S. R. Pendlebury, M. Cornuz, S. D. Tilley, M. Grätzel, J. R. Durrant, *J. Am. Chem. Soc.* **2014**, *136*, 2564.
- [95] O. Khaselev, J. A. Turner, *Science* **1998**, *280*, 425.
- [96] T. J. Jacobsson, V. Fjallstrom, M. Sahlberg, M. Edoff, T. Edvinsson, *Energy Environ. Sci.* **2013**, *6*, 3676.
- [97] J. Brillet, J. H. Yum, M. Cornuz, T. Hisatomi, R. Solaraska, J. Augustynski, M. Grätzel, K. Sivula, *Nat. Photonics* **2012**, *6*, 824.
- [98] S. Ida, K. Yamada, T. Matsunaga, H. Hagiwara, Y. Matsumoto, T. Ishihara, *J. Am. Chem. Soc.* **2010**, *132*, 17343.
- [99] P. Borno, F. F. Abdi, S. D. Tilley, B. Dam, R. van de Krol, M. Grätzel, K. Sivula, *J. Phys. Chem. C* **2014**, *118*, 16959.